Dyes and Pigments 219 (2023) 111630

Contents lists available at ScienceDirect

Dyes and Pigments

journal homepage: www.elsevier.com/locate/dyepig

A cyclometalated N-heterocyclic carbene and acetylacetonate ligands in a phosphorescent Pt(II) dye for sensing glucose

Irene Melendo [a], Javier Camacho-Aguayo [b], Sareh Paziresh [a], Sara Fuertes [a,***], Antonio Martín [a], Susana de Marcos [b], Javier Galbán [b,**], Violeta Sicilia [c,*]

[a] Departamento de Química Inorgánica, Facultad de Ciencias, Instituto de Síntesis Química y Catálisis Homogénea (ISQCH), CSIC - Universidad de Zaragoza, Pedro Cerbuna 12, 50009, Zaragoza, Spain

[b] Departamento de Química Analítica, Facultad de Ciencias, Instituto de Nanociencia y Materiales de Aragón (INMA), Universidad de Zaragoza, Pedro Cerbuna 12, 50009, Zaragoza, Spain

[c] Departamento de Química Inorgánica, Escuela de Ingeniería y Arquitectura de Zaragoza, Instituto de Síntesis Química y Catálisis Homogénea (ISQCH), CSIC - Universidad de Zaragoza, Campus Río Ebro, Edificio Torres Quevedo, 50018, Zaragoza, Spain

ARTICLE INFO

Keywords:
Glucose dye
Platinum (II)
Cyclometalated NHC
Acac
Phosphorescence

ABSTRACT

New β-diketonate platinum (II) complexes, containing a cyclometalated N-heterocyclic carbene [Pt(NaphˆC*$_{iPr}$)(acac)] (**3A**) (HNaphˆC*-κC* = 3-isopropyl-1-(naphthalen-2-yl)-1*H*-imidazole-2-ylidene), or a cyclometalated pyrazole, [Pt(NaphˆN$_{pz}$)(acac)] (**3B**) (HCˆN$_{pz}$ = 1-(naphthalen-2-yl)-*1H*-pyrazole) and [Pt(NaphˆN$_{dmpz}$)(acac)] (**3B'**) (HCˆN$_{dmpz}$ = 1-(naphthalen-2-yl)-*1H*-3,5-dimethylpyrazole) have been prepared and characterized. Their absorption and emission properties in films of ethyl cellulose (EC) were determined along with those of the already reported for complex [Pt(NaphˆC*$_{Me}$)(acac)] (**3A'**). They showed that all four β-diketonate complexes display a bright phosphorescent emission with maxima in the blue region (λ_{max} ~ 480 nm for **3A** and **3A'**; 490 nm **3B** and **3B'**). The higher quantum yield (QY), longer decay times and greater oxygen sensitivity were exhibited by the NaphˆC* derivatives, compared to the NaphˆN ones. Polyacrylamide membranes with entrapped **3A'** as dye, and glucose oxidase (GOx) enzyme were used for monitoring glucose level. The RSD is about 5% and the detection limit is at ~$5{\cdot}10^{-4}$ M, with a response time usually of 10–15 min working in stop-flow mode. These platinum-based membranes respond reversibly to glucose for, at least, 20 measures. **3A'** is the first Pt(II) complex bearing a cyclometalated N-heterocyclic carbene ever used as dye for sensing glucose.

1. Introduction

Phosphorescent transition metal complexes (TMCs), as those of Pt (II), became an interesting field of research. The reason lies in their challenging applications, since they can be used as photoactive materials in different kinds of light-emitting devices (phosphorescent organic light emitting diodes, PhOLEDs and light emitting cells, LECs), [1–4] photodynamic therapy [5,6] biolabeling [7,8] or optical sensors [9–12]. Among the latter, their use in the detection and quantification of glucose is one of the most important analytical tasks, with significance in areas such as medicine, biotechnology and biochemistry [11,12]. There are different kinds of methods for sensing glucose. A widely used approach is based on measuring the O_2 consumption during the oxidation of glucose caused by the action of enzymes, such as glucose oxidase (GOx).

$$\alpha\text{-}D\text{-glucose} + \text{GOx (FAD)} \rightarrow \text{D-glucono-1,5-lactone} + \text{GOx (FADH}_2\text{)} \quad \text{(eq.1)}$$

$$\text{GOx (FADH}_2\text{)} + O_2 \rightarrow \text{GOx (FAD)} + H_2O_2 \quad \text{(eq.2)}$$

Obviously, the concentration of glucose is related to the consumption of oxygen because of the enzymatic reaction. For that, these sensors use as probes TMCs whose phosphorescence is photophysically quenched by O_2. Considering the Stern-Volmer equation (eq. 3), which in its simple form reads as

$$\frac{I_0}{I} = \frac{\tau_0}{\tau} = 1 + K_{SV}[O_2] \quad \text{(eq.3)}$$

* Corresponding author.
** Corresponding author.
*** Corresponding author.
E-mail address: sicilia@unizar.es (V. Sicilia).

https://doi.org/10.1016/j.dyepig.2023.111630
Received 25 May 2023; Received in revised form 8 August 2023; Accepted 17 August 2023
Available online 18 August 2023

The sensitivity of a phosphorescent TMC to oxygen is higher the longer its decay time (τ_0) and emission intensity (I_0) in the absence of O_2 [9]. Typical probes for sensing glucose include ruthenium or platinum complexes, which can be excited with visible light. They possess large Stokes' shifts, long decay times and good photostability, [11] such as tris (bipyridine)ruthenium(II) ($[Ru(bpy)_3]^{2+}$), tris(1,10-phenantroline) ruthenium(II) ($[Ru(phen)_3]^{2+}$), tris(4,7-diphenyl-1,10-phenanthroline) ruthenium (II) ($[Ru(dpp)_3]^{2+}$), platinum(II) octaethylporphyrin (PtOEP) or platinum(II) octaethylketoporphyrin (PtOEPK) [13].

In the chemistry of platinum, new porphyrins [14] and mainly, new C,N-cyclometalated platinum (II) complexes have emerged as oxygen-probes, as those depicted in Scheme 1 (a), [15] (b), [16] (c), [17] (d), [18] (e), [19] (f), [20] (g) [21].

Compared to C,N-cyclometalated ligands, the use of cyclometalated N-heterocyclic carbenes (NHCs, C^C*) has been revealed as a key to get stable and very efficient Pt(II) phosphorescent emitters. The presence of two strong carbon-metal bonds induce high crystal field splitting, therefore reducing the photo- or thermal population of high-lying metal dd* states, which result in non-radiative deactivation and degradation via bond-breaking processes. They also confer robustness and stability and provide long-term functional materials [22]. For this work, we undertook the synthesis of new phosphorescent C^N and C^C* complexes of Pt(II) that contain a σ–bonded naphthyl group, with a large π–conjugation, in the chromophore, aiming to achieve long emission decay times, and acetylacetonate as auxiliary ligand. Our investigation on their luminescence in ethyl cellulose (EC) films showed higher emission efficiency and longer decay times for the C^C* derivatives compared to the C^N counterparts. The potential use of the formers as sensing probes for glucose was investigated.

2. Results and discussion

2.1. Synthesis and characterization

The synthetic routes for the new compounds, [Pt(Naph^C*$_{iPr}$)Cl (NCMe)] (**2A**) (HNaph^C*$_{iPr}$ = 3-isopropyl-1-(naphthalen-2-yl)-1*H*-imidazole-2-ylidene), [Pt(Naph^N$_{dmpz}$)Cl(NCMe)] (**2B'**) (HNaph^N$_{dmpz}$ = 1-(naphthalen-2-yl)-*1H*-3,5-dimethylpyrazole) and their intermediates (**A**, **1A**, **B'**, **1B'**) are illustrated in Scheme 2. All of them were prepared following the protocols [23,24] reported previously by our group and fully characterized. Compound **2B'** was prepared more efficiently by direct reaction of **B'** and [{Pt(η^3-2-Me-C_3H_4)(μ-Cl)}$_2$] [Pt], following path g in Scheme 2 (See Experimental Section and Figs. S1–S6 in Supporting Information).

Then, **2A** and **2B'** were used, along with the already reported **2B**, [23] as starting material for the synthesis of new acac derivatives (**3A**, **3B** and **3B'**), following the same protocol described for **3A'** [24].

The reactions of **2A, 2B** and **2B'** with Tl(acac) in 1.1 M ratio (Scheme 3) led to the precipitation of TlCl and formation of the neutral complexes [Pt(Naph^C*$_{iPr}$)(acac)] (**3A**), [Pt(Naph^N$_{pz}$)(acac)] (**3B**) and [Pt (Naph^N$_{dmpz}$)(acac)] (**3B'**) respectively. They were obtained as air-stable solids in good yields (See Experimental Section and Figs. S7–S9 in Supporting Information).

The presence of two ν_{st} (C═O) bands (range: 1550 - 1600 cm^{-1}) in their IR, and two methyl resonances in their ^{1}H NMR spectra (CD_2Cl_2, δ (ppm): 2.12 and 1.98 (**3A**); 2.07 and 2.00 (**3B**); 2.06 and 1.95 (**3B'**)), indicate the nonequivalence of the two halves of the acac ligand. They are in agreement with the chelate coordination of acac to platinum in complexes **3A, 3B** and **3B**', as observed for complex **3A'** [24].

The ^{195}Pt{^{1}H} NMR spectrum of **3A** in CD_2Cl_2 exhibits a singlet at −3356 ppm, which is very similar to the registered for **3A'** (−3360 ppm). Compounds **3B** (−2782 ppm) and **3B'** (−2757 ppm) exhibit also a singlet, which account for the purity of these samples. The downfield shift of the ^{195}Pt{^{1}H} signals in **3B** and **3B'** with respect to those in **3A** and **3A'**, points to a lower donor ability of the pyrazole fragments with respect to the carbene ones.

The single crystal X-ray structures of **3A** and **3B** showed that they are mononuclear neutral complexes with the Pt(II) center in a distorted square-planar environment due to the small bite angle of the cyclometalated ligand [~80°] (Fig. 1 and Table 1). The asymmetric unit for **3A** contains two molecules (Pt1 and Pt2) with similar structural details.

A O,O'-chelated acetylacetonate (acac) completes the Pt coordination sphere, with the angle O1–Pt–O2 close to 90° in all cases. The Pt–O bond distances are similar to those found in related β–diketonate complexes [24–27]. The Pt–O2 distances being the largest, complying with the C_{Naph} donor atom having a higher *trans* influence than that of C* and N_{pz}. Bond distances and angles corresponding to the Pt(Naph^C*) and Pt (Naph^N$_{pz}$) fragments are in the range of those observed in complexes with similar cyclometalated groups [23–25]. These complexes are almost planar, with a dihedral angle between the Pt(Naph^E) and Pt (acac) planes of about 3.7°. In their crystal packing, the molecules arrange in pairs, in a head to tail fashion. These dimers are held together through intermolecular Pt···Pt (~3.4 Å) and π···π (<3.5 Å) interactions between the Naph^C* ligand and the acac moiety for **3A**, as observed for **3A'** [24]. Likewise, in compound **3B**, they are held together by the existence of Pt···C5 (~3.4 Å, blue dotted line) and π···π (<3.5 Å, green dotted line) interactions between the Naph^N$_{pz}$ ligand and the acac moiety belonging to adjacent monomers. These contacts are only observed within the dimers and are not extended outside them.

2.2. Photophysical properties

The emission properties of the acac derivatives, [Pt(Naph^C*$_{iPr}$) (acac)] (**3A**), [Pt(Naph^C*$_{Me}$)(acac)] (**3A'**), [Pt(Naph^N$_{pz}$)(acac)] (**3B**) and [Pt(Naph^N$_{dmpz}$)(acac)] (**3B'**) in films of ethyl cellulose (wt % of compound: 2% and 20%) were investigated (see Table 2, and Fig. 2 and

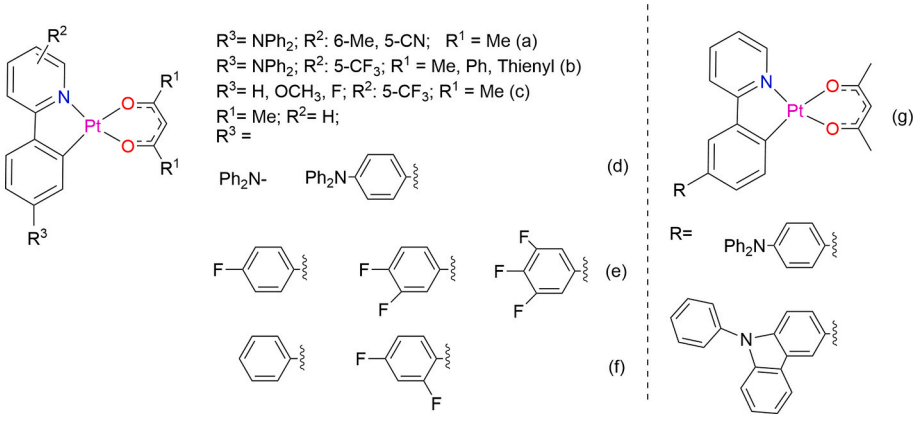

Scheme 1. Platinum C,N-cyclometalated complexes in optical sensors of oxygen.

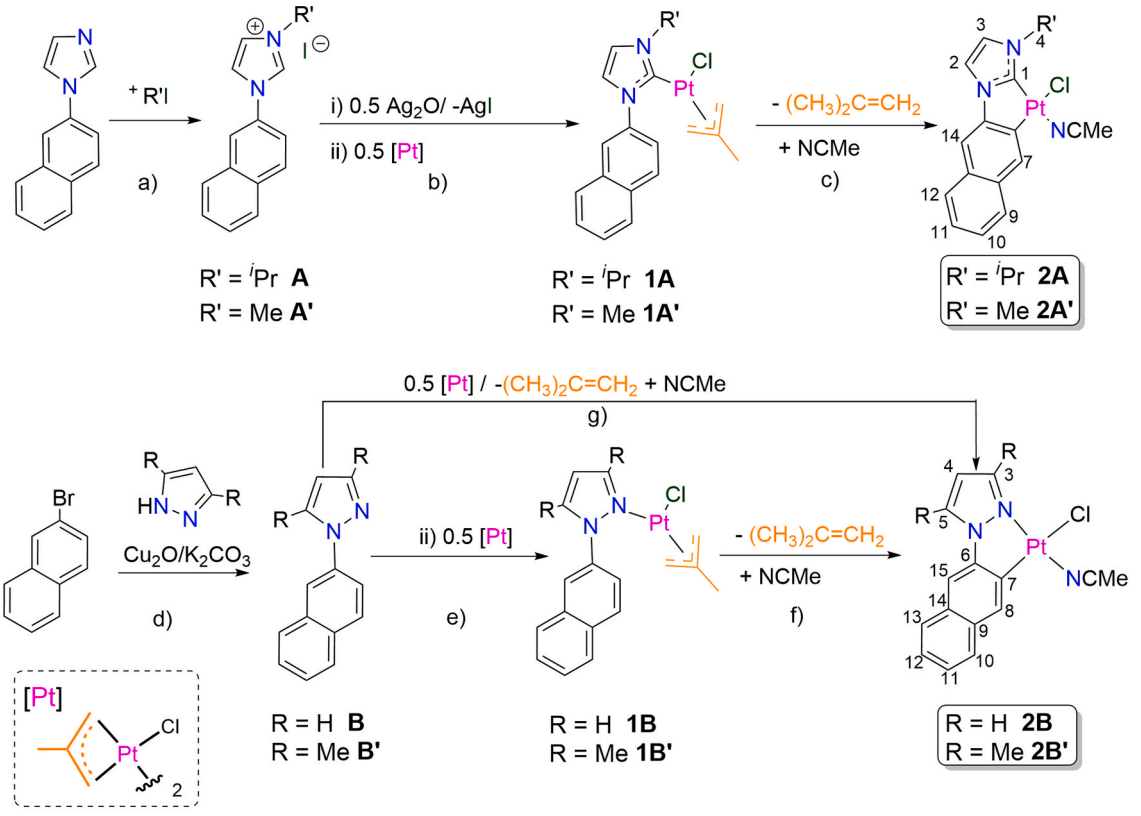

Scheme 2. Synthetic routes to achieve the starting materials **2A, 2A'**, **2B** and **2B**' and numerical scheme for NMR purposes.

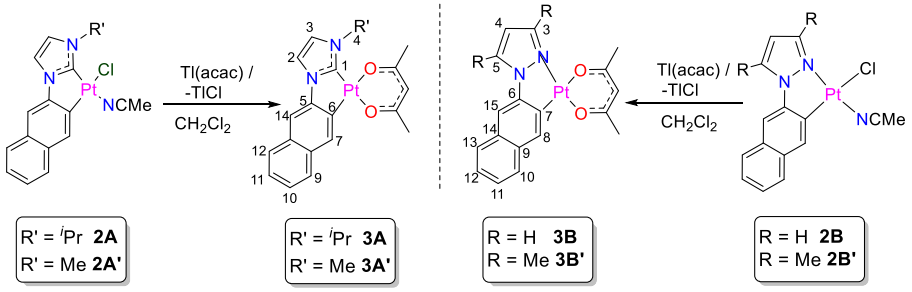

Scheme 3. Synthetic route to achieve complexes **3A, 3A'**, **3B** and **3B**' and numerical scheme for NMR purposes.

S10), prior to perform the sensing probes. They were compared with the already reported ones for compound [Pt(NaphˆC^*_{Me})(acac)] (**3A'**) in glassy 2-methyltetrahydrofuran (2-MeTHF) and powdery solid [24]. In EC films, the emission spectra of **3A** and **3A'** match each other (Fig. 2) like those of **3B** and **3B'** (Fig. S10) indicating that the difference in the R-substituents of the NaphˆC^* or NaphˆN scaffolds do not cause significant changes in the emission bands. In 2%wt films, upon excitation in the low-lying absorption region (λ: 350–380 nm), all the acac complexes display a bright phosphorescent emission with maxima in the blue region (λ_{max} ~ 480 nm for **3A** and **3A'**; 490 nm **3B** and **3B'**). In cases of **3A** and **3A'** their emissions match with that observed for **3A'** in diluted glassy solutions (10^{-5} M) of 2-MeTHF [24]. The structured shape of these bands, with vibrational spacings [1380- 1460 cm^{-1}] corresponding to the C═C/C═N stretches of the cyclometalated ligands (NaphˆE, E = C^*, N_{pz}) and their long decay times, point to the involvement of the NaphˆE ligands in the emissive state.

In all cases, the emission is characteristic of monomeric species. On the basis of the excitation spectra, that resemble the absorption ones (Table S2 and Figs. S11 and S12), and the TD-DFT calculations for **3A'**, [24] and **3B** (see in SI, Tables S3–S5), they could be attributed to mixed ^{3}ML'CT [5d(Pt)→π*(acac)]/^{3}LL'CT[π(NaphˆC^*)→π*(acac)]/^{3}IL transitions for **3A',** [24] while ^{3}ILCT [π(NaphˆN)→π*(NaphˆN)]/^{3}MLCT [5d(Pt)→π*(NaphˆN)] for **3B**.

20%wt EC films of **3A** and **3A'** show also structured emission bands, but red-shifted with respect to those at 2%wt, while no change was observed for the emissions of **3B** and **3B'** with concentration (Figs. S10a and S10b). These green-yellowish emission bands match with the emission of **3A**, [24] and NBu_4 [Pt(NaphˆC^*_{Me})$(CN)_2$] [28] in solid state, and appear to be less quenched by the presence of oxygen (Table 2).

Compared to the NaphˆN complexes (**3B** and **3B'**), higher QYs and longer decay times were measured for the NaphˆC^* derivatives (**3A** and **3A'**) in 2% wt films in EC, as can be seen in Table 2. These values resulted to be clearly more sensitive to the presence of O_2 than those of **3B** and **3B'**. Therefore, **3A** and **3A'** were selected as dyes for sensing

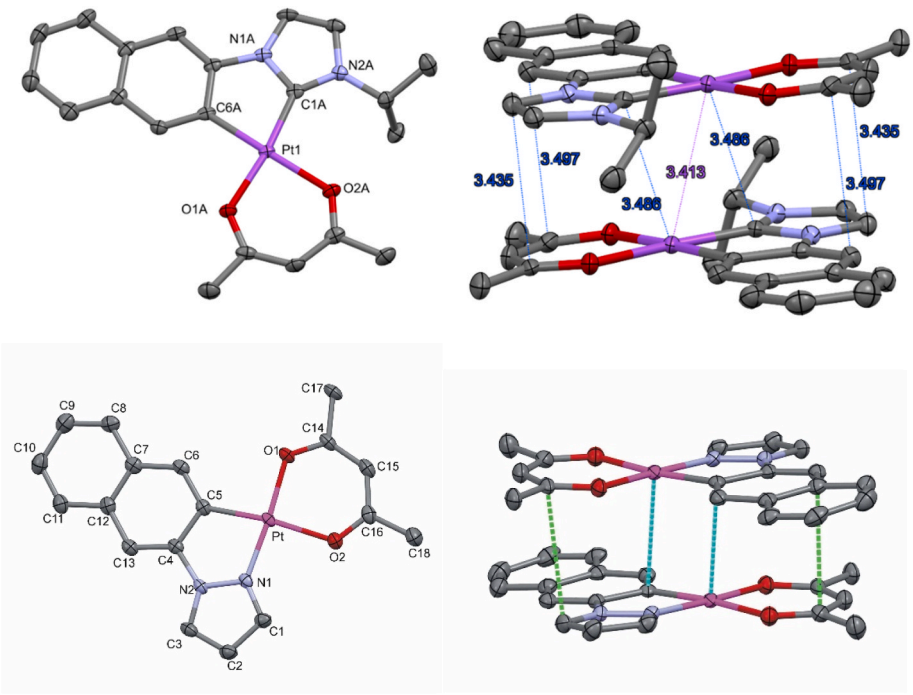

Fig. 1. Left: X-Ray structure of **3A (Pt1)** top and **3B** bottom; Right: stacking arrangement of **3A (Pt2)** top and **3B** bottom.

Table 1
Selected bond lengths (Å) and angles (°) for **3A** and **3B**.

Lengths (Å)	3A Pt(1) E = C*	3A Pt(2) E = C*	3B E = N
Pt-E	1.949(4)	1.958(4)	1.968(2)
Pt-C_{Naph}	1.982(4)	1.999(4)	1.978(3)
Pt–O1	2.059(2)	2.063(3)	2.0049(19)
Pt–O2	2.085(3)	2.092(3)	2.072(2)
Pt···Pt	3.426	3.413	
Angles (°)			
E-Pt-C_{Naph}	80.43(15)	81.22(16)	81.40(10)
O1–Pt–O2	89.84(10)	90.01(11)	92.79(8)
O1–Pt-C_{Naph}	92.04(13)	91.83(14)	94.08(10)
O2–Pt-E	97.66(13)	96.92(14)	91.73(9)

oxygen.

2.3. Oxygen and glucose sensing probes

Films of **3A** and **3A'** in EC 2%wt were used to evaluate their response to O_2 gas. They were placed in a homemade flow cell and gas was continuously pumped (Fig. 3).

The emission at λ_{em} = 480 nm (λ_{ex} = 350 nm) was monitored for different oxygen concentrations: 0% (N_2 atmosphere); 22% (Air); 100% (pure O_2). The results are represented in Figs. S13 and S14. As can be seen, the films are sensitive and reversible to O_2 gas, and as it has been previously reported, [9] a modified Stern–Volmer is required to study the quenching effect.

In order to broaden the applicability, it was also studied the response to dissolved oxygen in aqueous solutions. To do that, 2%wt EC films were coupled to the enzymatic reaction of glucose with Glucose Oxidase. The films were immersed in a fluorescence cuvette containing glucose oxidase (600 U/mL) in phosphate buffer pH 6 to which different glucose concentrations were added. The results appear listed in Tables S6 and S7 in the SI and in Fig. 4. As can be seen, in this case, the response fits to a Stern-Volmer of the type,

$$\frac{\mathbf{1}}{\mathbf{F}} = \frac{1}{F_0} + \frac{K_q}{F_0}[\mathbf{O_2}]$$

Corresponding to a static quenching effect of the oxygen in the luminescence of the **3A** and **3A'**films.

Going a step further, we decided to explore **3A'**, which exhibits brighter phosphorescence, as probe for sensing glucose. To do that, ground 2%wt film of **3A'** in EC was loaded and trapped inside a polyacrylamide gel membrane containing GOx. Then, phosphorescence measurements (λ_{ex} = 350 nm, λ_{em} = 480 nm) were performed for continuous monitoring of glucose, and the results appear represented in Fig. 5. All measurements (around 20) were performed with the same polyacrylamide glucose sensor and previous studies demonstrated that

Table 2
Emission data of **3A**, **3A'**, **3B** and **3B'** in EC films at 298 K.

Comp.	%wt in the Film	λ_{exc} (nm)	λ_{em} (nm)	τ (μs) Air/Ar	QY Air/Ar
3A	2	350	479_{max}, 515, 555, 600_{sh}	4/221	1/29
	20	380	481_{sh}, 532 $_{max}$, 575, 620_{sh}	15/20	4/10
3A'	2	350	478_{max}, 514, 554, 587	4.6/207	1/33
	20	380	535_{max}, 577, 626	27/30	40/60
3B[a]	2	360	492_{max}, 530, 572, 620_{sh}	5.3/155	0/12
3B'[a]	2	360	489_{max}, 526, 568, 615_{sh}	5/135	0.4/6.1

[a] Emission data at 20%wt match those at 2%wt.

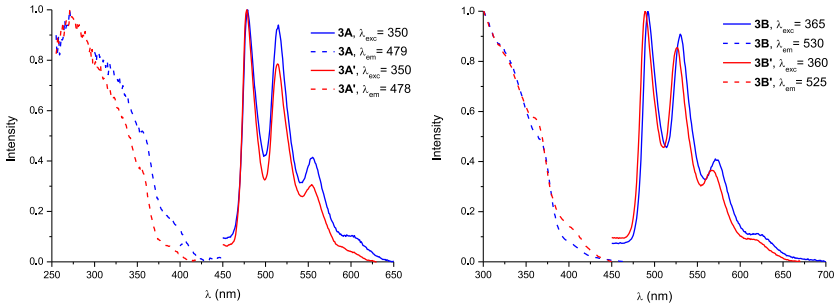

Fig. 2. Normalized excitation and emission spectra of **3A, 3A', 3B** and **3B'** in EC 2% wt.

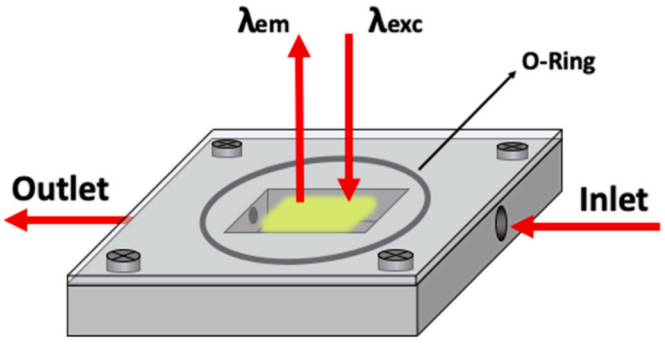

Fig. 3. Homemade flow cell.

the polyacrylamide gel containing Glucose Oxidase could be used for at least 100 times [29].

The sensor film shows a reversible response to glucose in the range from $1.0{\cdot}10^{-3}$ to $1.5{\cdot}10^{-2}$ M, but as it was expected, the sensitivity was lower than working in solution.

A higher sensitivity of this biosensor was achieved working in stop-flow mode. By stop pumping after the injection of each 2 mL of glucose solution into the system, phosphorescence measurements were performed for different concentrations of glucose. In this case, the sensor film shows a reversible response to glucose in the range from $5{\cdot}10^{-4}$ to $4{\cdot}10^{-3}$ M, with higher stability and faster-system regeneration (Fig. 6).

The sensitivity-range of this Pt-based biosensor ($5{\cdot}10^{-4}$- $4{\cdot}10^{-3}$ M) is enough for glucose blood levels analyses and comparable to that found for Gox polystyrene membranes based on PtOEPK [11,13].

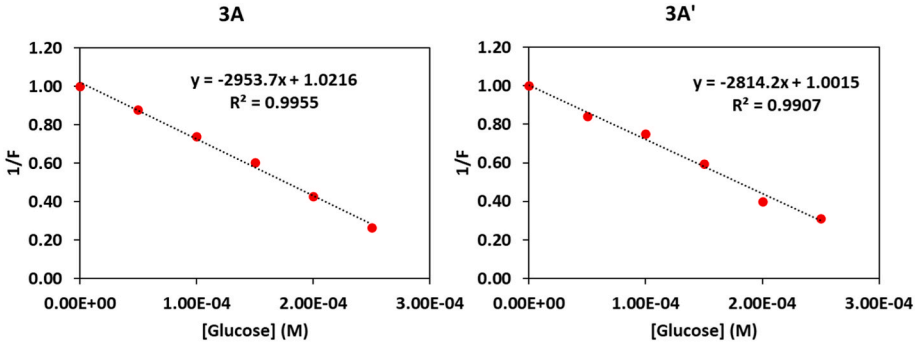

Fig. 4. Variation of the phosphorescence intensity (λ_{ex} = 350 nm, λ_{em} = 480 nm) for **3A** (left) and **3A'** (right) EC films (2%wt) in aqueous solution with the concentration of glucose.

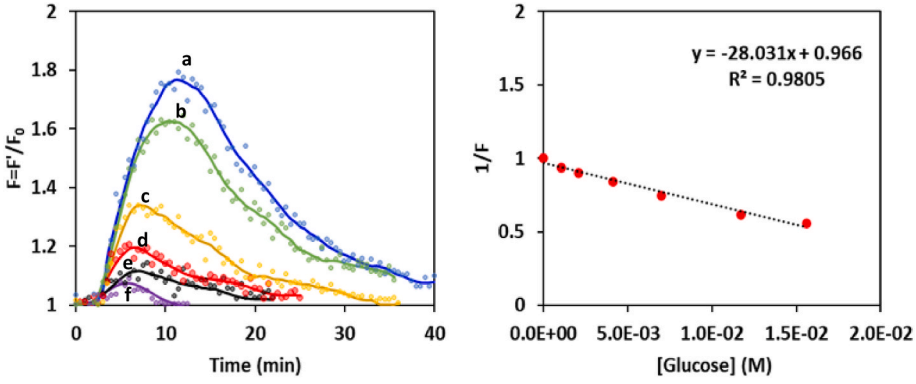

Fig. 5. Left: Continuous monitoring of the phosphorescence intensity (λ_{ex} = 350 nm, λ_{em} = 480 nm) for a **3A'** EC film (2%wt) entrapped in a GOx polyacrylamide biosensor film, with the concentration of glucose. Right. Stern- Volmer plot (1/F) for different glucose concentrations. a: $1.56{\cdot}10^{-2}$ M; b: $1.12{\cdot}10^{-2}$ M; c: $7.00{\cdot}10^{-3}$ M; d: $4.10{\cdot}10^{-3}$ M; e: $2.08{\cdot}10^{-3}$ M; f: $1.04{\cdot}10^{-3}$ M.

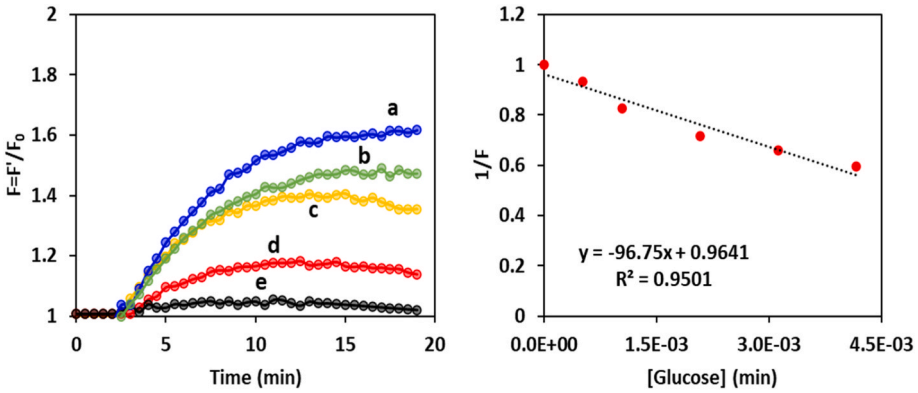

Fig. 6. Left: Variation of the phosphorescence intensity (λ_{ex} = 350 nm, λ_{em} = 480 nm), in stop-flow mode, for a **3A'** EC film (2%wt) entrapped in a GOx polyacrylamide biosensor film with the concentration of glucose. Right. Stern-Volmer plot (1/F) for different glucose concentrations. a: $4.16{\cdot}10^{-3}$ M; b: $3.12{\cdot}10^{-3}$ M; c: $2.08{\cdot}10^{-3}$ M; d: $1.04{\cdot}10^{-3}$ M; e: $5.2{\cdot}10^{-4}$ M.

3. Conclusions

Compounds [Pt(NaphˆC^*_{iPr})Cl(NCMe)] (**2A**) and [Pt(NaphˆN_{dmpz})Cl(NCMe)] (**2B'**) and their intermediates (**A**, **1A**, **B'**, **1B'**) were prepared following the step by step protocols described for their **A'** and **B** counterparts. Then, they were used as starting materials to get the acac derivatives: [Pt(NaphˆC^*_{iPr})(acac)] (**3A**) [Pt(NaphˆC^*_{Me})(acac)] (**3A'**) and [Pt(NaphˆN_{pz})(acac)] (**3B**) and [Pt(NaphˆN_{dmpz})(acac)] (**3B'**). The emission properties of **3A**, **3A'**, **3B** and **3B'** in 2% wt EC films revealed that the NaphˆC* complexes (**3A** and **3A'**) exhibit higher QYs and longer decay times than their NaphˆN counterparts (**3B** and **3B'**) and a greater sensitivity to the presence of O_2.

GOx and **3A'** were immobilized in a polyacrylamide membrane to determine glucose levels by analyzing the oxygen quench of luminescence. This biosensor showed the RSD of about 5%, reaching a detection limit at $\sim 5{\cdot}10^{-4}$ M. and the platinum dye is stable for at least 20 measures. While the sensitivity-range of this Pt(CˆC*)-based biosensor is comparable to that found for the PtOEPK-based one, it does represent encouraging results and a benchmark for cycloplatinated N-heterocyclic compounds. All this along with the good stability of Pt(CˆC*) materials open the door for long-term Pt-based glucose sensors.

4. Experimental section

4.1. Materials and general procedures

[{Pt(η^3-2-Me-C_3H_4)(μ-Cl)}$_2$], [30] 1-(naphthalen-2-yl)-1*H*-imidazole, [24] **A'**, [24] **1A'**, [24] **2A'**, [24] [Pt(NaphˆC^*_{Me})(acac)] (**3A'**), [24] **B**, [23] **1B**, [23] and [Pt(NaphˆN_{pz})Cl(NCMe)](**2B**) [23] were prepared following the literature procedures. Tl(acac) and silver(I) oxide were purchased from Strem; 2-bromonaphthalene, pyrazole and 3,5-dimethylpyrazole from Merck; imidazole and 2-iodopropane from Alfa Aesar and they were used as supplied. ^{1}H, ^{13}C{^{1}H} and ^{195}Pt{^{1}H} NMR spectra were recorded on Bruker 300 and 400 MHz instruments; the standard references were used: TMS for ^{1}H and ^{13}C and Na_2PtCl_6 in D_2O for ^{195}Pt. Coupling constants, *J*, are given in Hz and chemical shifts in ppm; assignments are based on ^{1}H–^{1}H COSY and ^{1}H–^{13}C HSQC and ^{1}H–^{13}C HMBC, ^{1}H–^{195}Pt HMQC experiments. Infrared spectra were recorded on Perkin-Elmer Spectrum 100 FT-IR and Jasco FT/IR-6600 spectrometers (ATR range 250–4000 cm^{-1}) as neat solids. Mass spectra were acquired using the matrix-assisted laser desorption ionization (MALDI) VG Autospec Bruker instrument. C, H, and N analyses were carried out in a Perkin-Elmer 2400 CHNS analyzer. UV–visible spectra were registered on a Unicam UV4 spectrophotometer. Steady-state photoluminescence spectra were recorded on a Jobin-Yvon Horiba Fluorolog FL-3-11 spectrofluorimeter. Phosphorescence lifetimes were recorded with a Fluoromax phosphorimeter accessory containing a UV xenon flash tube. Nanosecond lifetimes were recorded with a Datastation HUB-B with a nanoLED controller and software DAS6. Quantum yields were measured using the Hamamatsu Absolute PL Quantum Yield Measurement System C11347-11. EC films were prepared by dissolving 5×10^{-6} mol of the complex (**3A**, **3A'**) in 1 mL of dichloromethane ($5{\cdot}10^{-3}$ M). After that, EC (98% weight or 80% weight) was slowly added with vigorous stirring. The clear solutions were deposited on optical grade quartz plates of 1 × 1 cm by drop casting, and allowed to dry overnight before the measurements were carried out.

CCDC Nos. 2257278 and 2257279 contain the supplementary crystallographic data for **3A** and **3B**.

Glucose Oxidase (GOx) from Apergillus Niger, Type X–S, (EC 1.1.3.4) with an activity of 150.000 U·g^{-}1, Na_2HPO_4 (S9763) and Na_2PO_4 (S9638) for the buffer preparations and D-(+)-Glucose (G2870) were supplied by Sigma-Aldrich. Fluorescence measurements were made using an Agilent Fluorescence Spectrofotometer (Cary Eclipse).

The sensor support was prepared by dissolving 4 mg of GOx, 185 μL of a 30% acrylamide/N.N'-bis-acrylamide solution, 27 μL of a 10% (w/v) $(NH_4)_2S_2O_8$ and 3 μL of the commercial TEMED in 785 μL of TRIS buffer pH 6.

4.2. Synthesis of new precursors

4.2.1. 3-Isopropyl-1-(naphthalen-2-yl)-1H-imidazolium iodide (A)

2-iodopropane (0.2 mL, 2.32 mmol) was added to a solution of 1-(naphthalen-2-yl)-1*H*-imidazole (0.150 g, 0.77 mmol) in anhydrous CH_3CN (5 mL) under an Ar atmosphere. The resulting mixture was heated to reflux for 48 h. The solvent was removed in vacuum and cold THF (3 mL) was added to the residue. Then, the white solid was filtered and washed with cold THF (3 mL) and diethyl ether (5 mL) to give **A**. Yield: 0.270 g (81%). Anal. Found: C, 52.67; H, 4.60; N, 7.90. Molecular formula $C_{16}H_{17}N_2I$ requires: C, 52.76; H, 4.70; N, 7.69. ^{1}H NMR (300 MHz, DMSO-d_6): 9.93 (s, 1H, H_{im}); 8.47 (s, br, 1H, H_{im}); 8.43 (s, br, 1H, H_{14}); 8.24 (d, $^3J_{H\text{-}H}$ = 8.8, 1H, H_7); 8.21 (s, br, 1H, H_{im}); [8.13–8.01] (m, 2H, H_9, H_{12}); 7.94 (dd, $^3J_{H\text{-}H}$ = 8.8, $^4J_{H\text{-}H}$ = 2.1, 1H, H_6); [7.75–7.64] (m, 2H, H_{10}, H_{11}); 4.74 (sept, $^3J_{H\text{-}H}$ = 6.6, 1H, H_4); 1.59 (d, $^3J_{H\text{-}H}$ = 6.6, 6H, CH_3 ^{i}Pr).

4.2.2. [PtCl(η^3-2-Me-C_3H_4)(HNaphˆC^*_{iPr}-κC*)](1A)

Silver(I) oxide (0.086 g, 0.37 mmol) was added to a solution of **A** (0.270 g, 0.74 mmol) in anhydrous dichloromethane (20 mL) under an Ar atmosphere and in the dark. After 2.5 h stirring at r.t. [{Pt(η^3-2-Me-C_3H_4)(μ-Cl)}$_2$] (0.213 g, 0.37 mmol) was added to the mixture, which was allowed to react for 3.5 h. The yellow precipitate (AgI) was separated by filtration through Celite under Ar. The resulting yellow solution was evaporated to dryness and treated with anhydrous *n*-hexane (3 × 15 mL) to afford **1A** as a pale-yellow solid. Yield: 0.210 g (55%). Anal.

Found: C, 45.72; H, 4.51; N, 4.88. Molecular formula $C_{20}H_{23}ClN_2Pt$ requires: C, 46.02; H, 4.44; N, 5.37. ^{1}H NMR (300 MHz, CD_2Cl_2): 8.14 (s, 1H, H_{14}); [7.99–7.83] (m, 4H, H_6, H_7, $H_{naphthyl}$); [7.59–7.49] (m, 2H, $H_{naphthyl}$); 7.35 (d, $^3J_{H\text{-}H} = 2.0$, $^4J_{H\text{-}Pt} = 12.6$, 1H, H_{im}); 7.21 (d, $^3J_{H\text{-}H} = 2.0$, $^4J_{H\text{-}Pt} = 16.6$, 1H, H_{im}); 5.45 (m, 1H, H_4); 3.54 (d, $^2J_{H\text{-}H} = 2.7$, 1H, H_{allyl}); 2.59 (s, $^2J_{H\text{-}Pt} = 29.2$, 1H, H_{allyl}); 2.26 (s, $^2J_{H\text{-}Pt} = 30.3$, 1H, H H_{allyl}); 1.50 (d, $^3J_{H\text{-}H} = 6.8$, 6H, CH_3 ^{i}Pr). The CH_3 and one CH resonances of the allyl are overlapped with that of the water signal.

4.2.3. [Pt(Naph^C*$_{iPr}$)Cl(NCMe)] (2A)

Compound **1A** (0.212 g, 0.40 mmol) was dissolved in 2-methoxyethanol (12 mL) and heated to reflux for 4 h. After cooling down, the resultant grey suspension was filtered and the solid was washed with dichloromethane (2 × 5 mL) and diethyl ether (2 × 5 mL). The solid was recrystallized in hot MeCN (60 mL) and filtered through Celite. The solution was evaporated to dryness and *n*-hexane (4 × 15 mL) was added to the residue, to give **2A** as a pure white solid. Yield: 0.157 g (76%). Anal. Found: C, 42.14; H, 3.47; N, 8.03. Molecular formula $C_{18}H_{18}ClN_3Pt$ requires: C, 42.65; H, 3.58; N, 8.29. ^{1}H NMR (300 MHz, DMSO-d_6): 8.81 (s, $^3J_{H\text{-}Pt} = 61.4$, 1H, H_7); 8.25 (d, $^3J_{H\text{-}H} = 2.5$, H_{im}); 7.86 (s, $^3J_{H\text{-}Pt} = 14.1$, H_{14}); 7.79 (d, $^3J_{H\text{-}H} = 2.1$, H_{im}); 7.73 (d, $^3J_{H\text{-}H} = 7.6$, $H_{naphthyl}$); 7.66 (d, $^3J_{H\text{-}H} = 7.8$, $H_{naphthyl}$); [7.45–7.31] (m, 2H, H_{10}, H_{11}); 6.25 (sept, $^3J_{H\text{-}H} = 6.7$, 1H, H_4); 2.07 (s, 3H, CH_3 MeCN); 1.44 (d, $^3J_{H\text{-}H} = 6.7$, 6H, CH_3 ^{i}Pr). MS (MALDI+): 466.273 [Pt(Naph^C*$_{iPr}$)Cl]$^+$. IR (cm^{-1}): 281 (Pt–Cl).

4.2.4. 1-(2-naphthalenyl)-1H-3,5-dimethylpyrazole (HNaph^N$_{dmpz}$) (B')

A reaction mixture of 2-bromonaphthalene (0.670 g, 3.23 mmol), 3,5-dimethylpyrazole (0.466 g, 4.85 mmol), Cu_2O (0.055 g, 0.38 mmol), ^{t}BuONa (0.620 g, 6.46 mmol) and deoxygenated DMSO (6 mL) was stirred at 150 °C under Ar atmosphere for 72 h. The mixture was cooled at r.t. and ethyl acetate (60 mL) was added to it. Then it was filtered through Celites. The resulting solution was washed with distilled water (2 × 40 mL), and subsequently with a saturated aqueous solution of KCl (2 × 30 mL). The organic layer was separated and dried over $MgSO_4$; then it was evaporated to dryness resulting in blue-greenish oil.

The crude product was purified by column chromatography on silica gel using ethyl acetate/hexane (1:9) as eluent to give **B'** as a pure white solid. Yield: 0.320 g (44%). Anal. Found: C, 80.37; H, 6.50; N, 12.28. Molecular formula $C_{15}H_{14}N_2$ requires: C, 81.04; H, 6.35; N, 12.60. ^{1}H NMR (400 MHz, DMSO-d_6, δ):8.04–7.98] (m, 4H; H_8, H_{15}, H_{10}, H_{13}); 7.65 (dd,$^3J_{H\text{-}H} = 8$,$^4J_{H\text{-}H} = 2$, H_7); 7.61–7.54 (m, 2H; H_{11}, H_{12}); 6.09 (s, H_4); 2.35 (s, 3H; Me); 2.22 (s, 3H; Me).

4.2.5. [Pt(η^3-2-Me-C$_3$H$_4$)Cl(HNaph^N$_{dmpz}$-kN)] (1B')

Compound **B'** (0.066 g, 0.30 mmol) was added to a stirred solution of [{Pt(η^3-2-Me-C_3H_4)(μ-Cl)}$_2$] (0.0858 g, 0.15 mmol) in CH_2Cl_2 (6 mL) at r.t. After 1h, the solution was evaporated to dryness and n-hexane (5 mL) was added to the residue to give a yellow solid, which was filtered, washed with n-hexane (5 mL) and dried in the oven at 50 °C, **1B'**. Yield: 0.0946 g (62%). Anal. Found: C, 44.93; H, 4.16; N, 5.51. Molecular formula $C_{19}Cl_1H_{21}N_2Pt$ requires: C, 45.11; H, 4.29; N, 4.93. ^{1}H NMR (400 MHz, CD_2Cl_2, δ): 8.06–7.98 (m, 4H, H_8, H_{15}, H_{10}, H_{13}); 7.65–7.55 (m, 3H, H_7, H_{11}, H_{12}); 6.22 (s, 1H, H_4); 3.20 (m, $^2J_{Pt\text{-}H} = 28$, $1H_{syn}$, H_{allyl}); 3.03 (m, $^2J_{Pt\text{-}H} = 34.6$, $1H_{syn}$, H_{allyl}); 2.46 (s, 3H; Me); 2.23 (s, 3H; Me); 1.70 (m, $1H_{anti}$, H_{allyl}); 1.53 (s, 3H, Me, η^3-C_4H_7); 1.26 (m, $1H_{anti}$, H_{allyl}).

4.2.6. [Pt(Naph^N$_{dmpz}$)Cl(NCMe)] (2B')

[{Pt(η^3-2-Me-C_3H_4)(μ-Cl)}$_2$] (0.403 g, 0.70 mmol) was added to a solution of HNaph^N$_{dmpz}$ (**B'**) (0.312 g, 1.40 mmol) in 2-methoxyethanol (8 mL). The mixture was stirred for 30 min at r.t. and then, it was refluxed for 4 h. After cooling down to r.t., the resulting grey solid was filtered and washed with Et_2O (3 × 2 mL). The solid was recrystallized in refluxing MeCN (60 mL). The solution was evaporated to dryness and Et_2O (10 mL) added to the residue to give **2B'** as a pale-yellow solid. Yield: 0.374 g (54%). Anal. Found: C, 41.11; H, 3.24; N, 8.37. Molecular formula $C_{17}H_{16}ClN_3Pt$ requires: C, 41.43; H, 3.27; N, 8.52. ^{1}H NMR (300 MHz, DMSO-d_6, δ): 8.77 (s, $^3J_{Pt\text{-}H} = 54.7$, 1H, H_8); 7.91 (m, 2H, H_{10}, H_{15}); 7.68 (d, $^3J_{H\text{-}H} = 7.6$,1H, H_{13}); 7.46–7.37 (m, 2H; H_{11}, H_{12}); 6.45 (s,1H, H_4); 2.87 (s, 3H; Me); 2.70 (s, 3H; Me); 2.07 (s, 3H; MeCN). MS (MALDI+): 416.6 [Pt(Naph^N$_{dmpz}$)]$^+$; 452.6 [Pt(Naph^N$_{dmpz}$)Cl]$^+$. IR (cm^{-1}): 276 (Pt–Cl).

4.3. Synthesis of acac derivatives

4.3.1. [Pt(Naph^C*$_{iPr}$)(acac)] (3A)

Tl(acac) (0.180 g, 0.59 mmol) was added to a yellow suspension of **2A** (0.300 g, 0.59 mmol) in dichloromethane (50 mL) at r.t in the dark. After 4 h stirring, the resulting mixture was filtered through Celite and evaporated to dryness. Addition of methanol (3 × 5 mL) to the residue rendered a solid, which was recrystallized by redissolving in CH_2Cl_2/OEt_2 (1:1, 20 mL), filtering through Celite and evaporating to dryness. Addition of methanol (3 × 2 mL) to the residue rendered **3A** as a pure yellow solid. Yield: 0.212 g (67.8%). Anal. Found: C, 47.33; H, 3.97; N, 5.42. Molecular formula $C_{21}H_{22}N_2O_2Pt$ requires: C, 47.64; H, 4.19; N, 5.29. ^{1}H NMR (400 MHz, CD_2Cl_2, δ): 8.06 (s, $^3J_{H\text{-}Pt} = 56.6$, 1H, H_7); [7.80–7.75] (m, 1H, H_9); [7.74–7.69] (m, 1H, H_{12}); 7.46 (d, $^3J_{H\text{-}H} = 2.2$, 1H, H_2); 7.36 (s, 1H, H_{14}); [7.35–7.30] (m, 2H, H_{10}, H_{11}); 7.07 (d, $^3J_{H\text{-}H} = 2.2$, 1H, H_3); 5.70 (sept, $^3J_{H\text{-}H} = 6.7$, 1H, H_4); 5.57 (s, 1H, CH, acac); 2.12 (s, 3H, CH_3, acac); 1.98 (s, 3H, CH_3, acac); 1.51 (d, $^3J_{H\text{-}H} = 6.7$, 6H, CH_3 ^{i}Pr). ^{13}C{^{1}H} NMR plus HMBC and HSQC (100.6 MHz, CD_2Cl_2, δ): 185.6 (s, 2C, C═O, acac); 149.6 (s, C_1); 146.7 (s, C_5); 132.0, 131.9 (s, 2C, C_{13}, C_8); 129.8 (s, C_7); 127.6 (s, C_{12}); 127.3 (s, C_9); 125.1, 124.6 (s, 2C, C_{11}, C_{10}); 116.6 (s, C_3); 114.8 (s, C_2); 106.8 (s, $^3J_{C\text{-}Pt} = 32.5$, C_{14}); 102.1 (s, $^3J_{C\text{-}Pt} = 56.6$, CH, acac); 49.2 (s, C_4); 28.1 (s, CH_3, acac); 28.0 (s, CH_3, acac); 23.4 (s, 2C, CH_3 ^{i}Pr). ^{195}Pt{^{1}H}-NMR (85.6 MHz, CD_2Cl_2): –3356 (s). MS (ESI+, MeCN): 552.12 [Pt(Naph^C*$_{iPr}$)(acac)Na]$^+$.IR (cm^{-1}): 1558 and 1577 (C═O, acac).

4.3.2. [Pt(Naph^N$_{pz}$)(acac)] (3B)

Tl(acac) (0.1961 g, 0.65 mmol) was added to a suspension of [Pt(Naph^N$_{pz}$)Cl(NCMe)] (0.300 g, 0.65 mmol) in dichloromethane (40 mL) at r.t in the dark. After 3 h stirring, the resulting mixture was filtered through Celite and evaporated to dryness. Addition of methanol (3 × 5 mL) to the residue rendered a solid, which was recrystallized by redissolving it in dichloromethane/diethyl ether (2:1, 30 mL), filtering through Celite and evaporating to dryness. Addition of methanol (3 × 3 mL) to the residue rendered **3B** as a pure yellow solid. Yield: 135.7 mg (43.1%). Anal. Found: C, 43.83; H, 3.42; N, 5.67. Molecular formula $C_{18}H_{16}N_2O_2Pt$ requires: C, 44.08; H, 3.90; N,5.71. ^{1}H NMR (400 MHz, CD_2Cl_2, δ): 8.17 (d, 1H, $^3J_{H\text{-}H} = 2.8$, H_{pz}), 7.88 (d, 1H, $^3J_{H\text{-}H} = 2.3$, H_{pz}), 7.84 (s, 1H, H_7), 7.82–7.75 (m, 2H, H_9, H_{12}), 7.60 (s, 1H, H_{14}), 7.39 (m, 2H, H_{10}, H_{11}), 6.6 (dd, 1H, H_{pz}), 5.55 (s, 1H, CH, acac), 2.07 (s, 3H, Me, acac), 2.0 (s, 3H, Me, acac). ^{13}C{^{1}H} NMR plus HMBC and HSQC (101 MHz, CD_2Cl_2, δ): 186.3 (s, 1C, C═O, acac), 184.1 (s, 1C, C═O, acac), 137.9 (s, 1C, C_{pz}), 129.8 (s, C_7), 127.9, 127.3 (s, 2C, C_9, C_{12}), 125.7, 125.1 (s, 2C, C_{11}, C_{10}), 126.4 (s, 1C, C_{pz}), 107.5 (s, C_{pz}), 107.2 (s, C_{14}), 102.6 (s, $^3J_{C\text{-}Pt} = 65.9$, CH, acac), 27.9 (s, CH_3, acac), 27.1 (s, CH_3, acac). ^{195}Pt{^{1}H}-NMR (85.6 MHz, CD_2Cl_2): –2782 (s). MS (MALDI): *m/z* 487 [Pt (Naph^N$_{pz}$)(acac)]. IR (cm^{-1}): 1512 and 1560 (C═O, acac).

4.3.3. [Pt(Naph^N$_{dmpz}$)(acac)] (3B')

Tl(acac) (0.124 g, 0.41 mmol) was added to a yellow solution of **2B'** (0.201 g, 0.41 mmol) in dichloromethane (40 mL) at r.t. and the mixture stirred for 4 h in the dark. The resulting mixture was filtered through

Celite and evaporated to dryness. Addition of methanol (3 × 5 mL) to the residue rendered a solid, which was recrystallized by redissolving in dichloromethane/diethyl ether (1:1, 20 mL), filtering through Celite and evaporating to dryness. Addition of methanol (3 × 5 mL) to the residue afforded **3B'** as a pure white solid. Yield: 108.8 mg (51.8%). Anal. Found: C, 46.22; H, 3.77; N, 5.12. Molecular formula $C_{20}H_{20}N_2O_2Pt$ requires: C, 46.60; H, 3.91; N, 5.43. ^{1}H NMR (400 MHz, CD_2Cl_2, δ): 7.86 (s, 1H, H_8); 7.82–7.75 (m, 2H, H_{10}, H_{13}); 7.60 (s, 1H, H_{15}); 7.39–7.33 (m, 2H, H_{11}, H_{12}); 6.10 (s, 1H, H_4); 5.56 (s, 1H, CH, acac); 2.80 (s, 3H, Me, C^N); 2.62 (s, 3H, Me, C^N); 2.06 (s, 3H, Me, acac); 1.95 (s, 3H, Me, acac). ^{13}C-{^{1}H} NMR (400 MHz, CD_2Cl_2, δ): 185.8, 183.9 (s, 2C, CO, acac); 152.7 (s, C_3); 145.3 (s, C_7); 141.0 (s, C_5); 131.8 and 131.0 (s, 2C, C_9 and C_{14}); 129.1(s, C_8); 128.1 and 127.1 (s, 2C, C_{10} and C_{13}); 125.4 and 124.7 (s, 2C, C_{11} and C_{12}); 120.8 (s, C_6); 110.3 (s, C_4); 108.1 (s, C_{15}); 102.0 (s, $C_{2'}$); 27.8 (s, Me, acac); 27.3 (s, Me, acac); 14.7 (s, Me, C^N); 12.1 (s, Me, C^N). ^{195}Pt{^{1}H}-NMR (85.6 MHz, CD_2Cl_2): – 2757 (s). MS (MALDI+): 515.4 [Pt(Naph^N_{dmpz})(acac)]$^+$. IR (cm^{-1}): 1522, 1578 (C═O, acac).

4.4. Sensing measurement procedures

4.4.1. Oxygen in gas phase

3A and **3A'** films were placed in a home-made flow cell, and oxygen, air or nitrogen were continuously pumped.

4.4.2. Glucose in solution

3A' in EC film (2%wt) was placed in a 1-cm fluorescence cell where it was added 300 U/mL of Glucose Oxidase in phosphate buffer pH 6. After stabilization, 20 μL of glucose of different concentrations were added and the variation of the phosphorescence (λ_{ex} = 350 nm, λ_{em} = 480 nm) was registered.

4.4.3. Glucose biosensor

3A' in EC film (2%wt) was trapped in a polyacrylamide GOx-sensor film and placed in a home-made flow cell. Glucose of different concentrations were pumped at 1 mL/min and the phosphorescence variation was registered at λ_{ex} = 350 nm, λ_{em} = 480 nm.

CRediT authorship contribution statement

Irene Melendo and Sareh Paziresh, are involved in the synthesis of compounds and photoluminescence measurements Antonio Martín is involved in X-ray determinations Sara Fuertes, and Violeta Sicilia are responsible for the conceptualization of the project, for writing, reviewing and editing the manuscript. Javier Camacho-Aguayo, Susana de Marcos, Javier Galbán are involved in the sensing of glucosa.

Declaration of competing interest

Authors declare that there are not conflict of interest.

Data availability

Scopus

Acknowledgment

This work was supported by the Spanish Ministerio de Ciencia Innovacion y Universidades/FEDER (Projects PID2021-122869NB-I00 and PID2019-105408GB-I00), by the Gobierno de Aragon (Grupos E17_20R: Química Inorgánica y de los Compuestos Organometálicos, and E25_20R: Nanosensores y Sistemas Bioanalíticos) J. Camacho-Aguayo thanks the Government of Aragón for a grant. The authors thank the Centro de Supercomputación de Galicia (CESGA) for generous allocation of computational resources.

Appendix A. Supplementary data

Supplementary data to this article can be found online at https://doi.org/10.1016/j.dyepig.2023.111630.

References

[1] Cebrian C, Mauro M. Recent advances in phosphorescent platinum complexes for organic light-emitting diodes. Beilstein J Org Chem 2018;14:1459–81.
[2] Weber KT, Karikis K, Weber MD, Coto PB, Charisiadis A, Charitaki D, Charalambidis G, Angaridis P, Coutsolelos AG, Costa RD. Cunning metal core: efficiency/stability dilemma in metallated porphyrin based light-emitting electrochemical cells. Dalton Trans 2016;45:13284–8.
[3] Shafikov MZ, Daniels R, Pander P, Dias FB, Williams JAG, Kozhevnikov VN. Dinuclear design of a Pt(II) complex affording highly efficient red emission: photophysical properties and application in solution-processible OLEDs. ACS Appl Mater Interfaces 2019;11:8182–93.
[4] Shafikov MZ, Tang S, Larsen C, Bodensteiner M, Kozhevnikov VN, Edman L. An efficient heterodinuclear Ir(III)/Pt(II) complex: synthesis, photophysics and application in light-emitting electrochemical cells. J Mater Chem A 2019;7:10672–82.
[5] Jain A. Multifunctional, heterometallic ruthenium-platinum complexes with medicinal applications. Coord Chem Rev 2019;401:213067.
[6] Zhong Y-F, Zhang H, Mu G, Liu W-T, Cao Q, Tan C-P, Ji L-N, Mao Z-W. Nucleus-localized platinum(II)–triphenylamine complexes as potent photodynamic anticancer agents. Inorg Chem Front 2019;6:2817–23.
[7] Mitra K, Lyons CE, Hartman MCT. A platinum(II) complex of heptamethine cyanine for photoenhanced cytotoxicity and cellular imaging in near-IR light. Angew Chem, Int Ed Engl 2018;57:10263–7.
[8] Law AS, Lee LC, Yeung MC, Lo KK, Yam VW. Amyloid protein-induced supramolecular self-assembly of water-soluble platinum(II) complexes: a luminescence assay for amyloid fibrillation detection and inhibitor screening. J Am Chem Soc 2019;141:18570–7.
[9] Wang X-D, Wolfbeis OS. Optical methods for sensisng and imaging oxygen: materials, spectroscopies and applications. Chem Soc Rev 2014;43:3666–761.
[10] Shigeta Y, Kobayashi A, Yoshida M, Kato M. Stability tuning of vapor-adsorbed state of vapochromic Pt(II) complex by introduction of chiral moiety. Inorg Chem 2019;58:7385–92.
[11] Steiner M-S, Duerkop A, Wolfbeis OS. Optical methods for sensing glucose. Chem Soc Rev 2011;40:4805–39.
[12] Choudhury B, Shinar R, Shinar J. Glucose biosensors based on organic light-emitting devices structurally integrated with a luminescent sensing element. J Appl Phys 2004;96:2949–54.
[13] Papkovsky DB, Ovchinnikov AN, Ogurtsov VI, Ponomarev GV, Korpela T. Biosensors on the basis of luminescent oxygen sensor: the use of microporous light-scattering support materials. Sens Actuators, B 1998;51:137–45.
[14] Manathanath M, Xie M, Arunkumar C, Wang Z, Zhao J, Sujatha S. Synthesis, photophysical, electrochemical and photoluminescent oxygen sensing studies of trans-Pt(II)-porphyrins. Dyes Pigments 2019;165:117–27.
[15] Liu C, Song XL, Rao XF, Xing Y, Wang ZG, Zhao JZ, Qiu JS. Novel triphenylamine-based cyclometalated platinum(II) complexes for efficient luminescent oxygen sensing. Dyes Pigments 2014;101:85–92.
[16] Yan YY, Yu ZN, Liu C, Jin X. Effects of phenyl/thienyl substituents at acetylacetone auxiliary ligands on the properties of cyclometalated platinum(II) complexes. Dyes Pigments 2020;173:107949.
[17] Xing Y, Liu C, Song XL, Li JY. Photostable trifluoromethyl-substituted platinum(II) emitters for continuous monitoring of molecular oxygen. J Mater Chem C 2015;3:2166–74.
[18] Wu WT, Cheng CH, Wu WH, Guo HM, Ji SM, Song P, Han KL, Zhao JZ, Zhang X, Wu YB, Du GT. Tuning the emission colour of triphenylamine-capped cyclometallated platinum(II) complexes and their application in luminescent oxygen sensing and organic light-emitting diodes. Eur J Inorg Chem 2010:4683–96.
[19] Xing Y, Liu C, Xiu JH, Li JY. Photostable fluorophenyl-substituted cyclometalated platinum(II) emitters for monitoring of molecular oxygen in real time. Inorg Chem 2015;54:7783–90.
[20] Xing Y, Wang L, Liu C, Jin X. Effects of fluorine and phenyl substituents on oxygen sensitivity and photostability of cyclometalated platinum(II) complexes. Sens Actuators B Chem 2020;304:127378.
[21] Di L, Xia Z, Wang H, Xing Y, Yang Z. Switchable and adjustable AIE activity of Pt (II) complexes achieving swift-responding and highly sensitive oxygen sensing. Sens Actuators, B 2021;326:128987.
[22] Amouri H. Luminescent complexes of platinum, iridium, and coinage metals containing N-heterocyclic carbene ligands: design, structural diversity, and photophysical properties. Chem Rev 2023;123:230–70.
[23] Paziresh S, Sicilia V, Ara I, Martín A, Fuertes S. The influence of cyclometalated ligand motifs on the solid-state assemblies and luminescent properties of Pt(II)-Tl (I) complexes. Organometallics 2019;38:3804–15.
[24] Fuertes S, García H, Perálvarez M, Hertog W, Carreras J, Sicilia V. Stepwise strategy to cyclometallated PtII complexes with N-heterocyclic carbene ligands: a luminescence study on new β-diketonate complexes. Chem Eur J 2015;21:1620–31.
[25] Fuertes S, Chueca AJ, Martín A, Sicilia V. Pt_2Tl building blocks for two-dimensional extended solids: synthesis, crystal structures, and luminescence. Cryst Growth Des 2017;17:4336–46.

[26] Strassner T. Phosphorescent platinum(II) complexes with C^C* cyclometalated NHC ligands. Acc Chem Res 2016;49:2680–9.
[27] Soellner J, Strassner T. Diaryl-1,2,3-Triazolylidene platinum(II) complexes. Chem Eur J 2018;24:5584–90.
[28] Ogawa T, Sameera WMC, Saito D, Yoshida M, Kobayashi A, Kato M. Phosphorescence properties of discrete platinum(II) complex anions bearing N-heterocyclic carbenes in the solid state. Inorg Chem 2018;57:14086–96.
[29] Sanz V, de Marcos S, Galbán J. A blood-assisted optical biosensor for automatic glucose determination. Talanta 2009;78:846–51.
[30] Mabbott DJ, Mann BE, Maitlis PM. Cationic (η-3-allylic) (η -4-diene)-Palladium and (η -4-diene)-Platinum complexes. J Chem Soc Dalton Trans 1977:294–9.